Contemporary Mathematics
https://ojs.wiserpub.com/index.php/CM/

Research Article

Discrete Fractional Order Modeling of Plant Capture Carbon Dioxide Dynamical Analysis with Neural Networking

Aziz Khan[1*], Hadeel Bin Amer[2], Thabet Abdeljawad[1], Rajermani Thinakaran[3]

[1] Department of Mathematics and Sciences, Prince Sultan University, Riyadh 11586, Saudi Arabia
[2] Department of Computer Science, College of Computer and Information Sciences, Majmaah University, Al-Majmaah 11952, Saudi Arabia
[3] Faculty of Data Science and Information Technology, INTI International University, Negeri Sembilan, Malaysia
E-mail: akhan@psu.edu.sa

Received: 25 November 2025; **Revised:** 28 January 2026; **Accepted:** 27 March 2026

Abstract: A nonlinear mathematical model is suggested to examine the role of varying abilities of plants in absorbing atmospheric Carbon Dioxide (CO_2) and its impact on the ecosystem. Various plant species show distinct abilities to absorb and capture CO_2, which can affect the overall reduction in atmospheric CO_2 quantities. The study objectives to consider how differences in plant capacities for CO_2 absorption influence atmospheric CO_2 levels. The focus is on identification the impact of plant growth rates and reaping rates on CO_2 concentration. The model is formulated using a difference operator to facilitate numerical exploration. It employs the Discrete Numerical Iterative Method (DNIM) joint with neural networks, particularly the Levenberg-Marquardt (LM) algorithm, known as DNIM-LM. The model's performance, training status, error distribution, regression, and suitability are calculated using artificial intelligence procedures. The dataset is split into 70% for training, 15% for authentication, and 15% for testing. The analysis shows that plants with higher CO_2 absorption capacities attain faster reductions in atmospheric CO_2 quantities as their growth rate increases. On the other hand, an increase in the harvesting rate coefficient is related to an increase in CO_2 concentration. The study determines that variations in plant absorption capacities expressively influence the dynamic contrast of atmospheric CO_2 reduction in the environment. This finding highlights the importance of plant growth rates and harvesting performs in managing CO_2 levels, present insights into ecosystem management and carbon sequestration policies.

***Keywords*:** difference operator, Discrete Numerical Iterative Method (DNIM), neural networks, Levenberg-Marquardt (LM), fit analysis

MSC: 26A33, 34A08, 03C65

1. Introduction

Global warming is a critical issue that needs immediate attention. Carbon Dioxide (CO_2) is the primary provider of global warming, and its abandoned accumulation can have lasting and permanent effects. The buildup of CO_2 in the atmosphere indicates higher global temperatures, which in turn results in extreme weather patterns, increasing sea levels, and a loss of biodiversity. To combat the mounting levels of global warming, it is important to reduce atmospheric CO_2,

Copyright ©2026 Aziz Khan, et al.
DOI: https://doi.org/10.37256/cm.7320269264
This is an open-access article distributed under a CC BY license
(Creative Commons Attribution 4.0 International License)
https://creativecommons.org/licenses/by/4.0/

[1]. One nominal method to accomplish this is by planting new forests. Forests help as natural carbon sinks, as they capture CO_2 from the air and accumulate it in their biomass and soil. By expanding the number of forested areas, we can improve this natural absorption manner, serving to counterbalance discharges from human activities. While not a complete solution, this approach is an essential part of a comprehensive methodology for mitigating climate change and guaranteeing environmental health [2]. From 2000–2020, global CO_2 emissions substantially increased, rising from approximately 25 gigatons to over 36 gigatons each year. This 44% rise has been driven primarily by the burning of fossil fuels for energy, industrial processes, and deforestation. During this period, the global average temperature increased by approximately 0.4 degrees Celsius, increasing the frequency and intensity of natural disasters such as droughts, hurricanes, and wildfires [3]. For example, 2016 was recorded as the warmest year, with temperatures nearly 1.2 degrees Celsius above preindustrial levels. This movement highlights the urgency of implementing nominal carbon mitigation strategies. Forests are important in this context because they can sequester momentous amounts of CO_2, [4]. According to the Food and Agriculture Organization (FAO), the world's forests captured approximately 2.4 gigatons of CO_2 annually from 2000–2020, offsetting approximately one-third of annual fossil fuel discharges. Nonetheless, deforestation and forest degradation have also been substantial, particularly in tropical regions [5]. The Amazon rain forest, for example, has experienced an annoying increase in deforestation levels, with an approximately 20% of its area lost over the last 50 years. The loss of these forests not only decreases the planet's capacity to capture CO_2 but also discharges stored carbon back into the atmosphere, contributing to global warming, [6]. Reforestation and afforestation methods can reverse some of these trends, Figure 1. Between 2000 and 2020, countries such as China and India carried out large-scale tree-planting strategies.

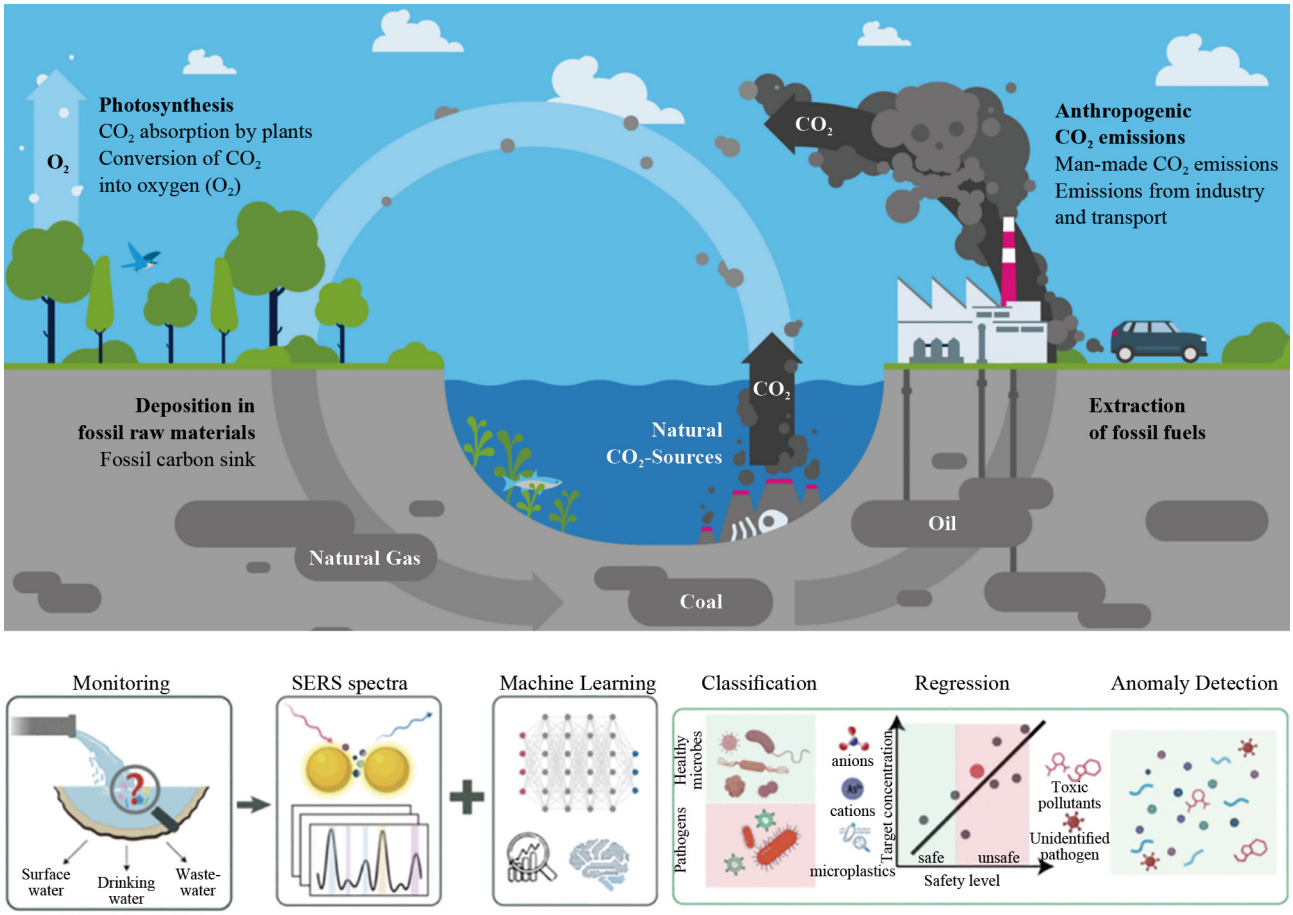


Figure 1. Plant absorption of CO_2

China's "Great Green Wall" scheme, aimed at combating desertification, led to the planting of more than 66 billion trees, [7]. This program alone has contributed substantially to global carbon appropriation efforts. Likewise, India's Green India Mission aims to increase forest and tree cover to restore tarnished ecosystems and enhance carbon sinks [8]. However, it is not sufficient to simply plant trees; the quality and diversity of these new forests are essential. Monoculture plantations, which are often employed for commercial determinations, do not provide the same environmental assistance as biodiverse forests do. Native species should be prioritized in reforestation plans to create resilient ecosystems that maintain a wide range of biodiversity. Furthermore, protecting existing forests from deforestation is correspondingly important. Efforts such as the Reducing Emissions from Deforestation and Forest Degradation (REDD+) platform incentivize developed countries to preserve their forests by providing financial and technical support [9].

Table 1. Top 10 countries CO_2 emissions (in million metric tons) from 2000–2020 [10, 11]

Year	China	USA	India	Russia	Japan	Germany	South Korea	Canada	Iran	Saudi Arabia
2000	3,311	5,790	1,018	1,482	1,229	822	438	598	568	377
2001	3,621	5,908	1,164	1,546	1,258	847	458	626	606	396
2002	4,036	5,975	1,242	1,561	1,279	842	469	629	639	429
2003	4,526	6,112	1,313	1,609	1,347	844	481	645	672	458
2004	5,113	6,381	1,377	1,621	1,385	830	489	646	701	490
2005	5,862	6,573	1,452	1,644	1,428	834	506	659	748	505
2006	6,459	6,719	1,546	1,665	1,485	845	526	676	803	530
2007	7,129	6,931	1,638	1,685	1,542	835	542	692	860	566
2008	7,448	6,802	1,721	1,680	1,482	813	540	676	889	572
2009	7,108	6,349	1,785	1,575	1,429	759	511	655	866	588
2010	7,687	6,865	1,887	1,604	1,489	764	537	665	919	614
2011	8,223	7,109	1,976	1,708	1,493	756	543	684	945	631
2012	8,568	7,115	2,049	1,719	1,466	734	541	688	965	640
2013	9,225	7,081	2,146	1,735	1,451	711	551	681	986	663
2014	9,462	7,105	2,263	1,728	1,440	697	567	663	983	686
2015	9,509	6,924	2,345	1,709	1,391	693	580	660	935	705
2016	9,233	6,892	2,415	1,678	1,362	684	578	644	931	733
2017	9,707	6,734	2,511	1,667	1,383	675	585	641	907	739
2018	9,890	6,646	2,629	1,628	1,381	677	597	639	906	751
2019	10,068	6,586	2,722	1,606	1,367	661	604	644	926	762
2020	9,672	5,416	2,523	1,558	1,298	612	589	629	797	757

A mathematical model using the difference operator can be instrumental in evaluating CO_2 emission and absorption dynamics. This method involves computing the discrete changes in CO_2 levels over time, providing a clearer picture of temporal variations [12]. By describing emission and absorption as distinct variables, the difference operator can track their particular increments or decrements between successive time intervals [13]. This methodology allows the identification of patterns, trends, and anomalies in CO_2 data, enabling a more precise consideration of the carbon cycle [14]. Additionally, the model can improve its accuracy by including factors such as deforestation, industrial activities, and reforestation [15].

The difference operator's ability to handle discrete data points makes it particularly suitable for environmental studies, where continuous monitoring and periodic data assortment are common. Therefore, this mathematical model can aid in enhancing more effective tactics for managing and mitigating CO_2 emissions, ultimately contributing to efforts to combat climate change [16]. By utilizing the difference operator, researchers and representatives can gain valuable perceptions of the efficacy of current measures and identify areas needing advancement, confirming that resources are optimally allocated to achieve the greatest environmental impact [17]. Artificial Intelligence (AI) has been increasingly engaged in analyzing and predicting CO_2 emissions and observations, incorporating its ability to process vast amounts of data and recognize patterns that traditional procedures might overlook [18]. A key feature of AI's application in this domain is its procedure of difference operators, which are mathematical tools applied to measure the changes or differences among data points [19]. In the framework of CO_2 emissions, a difference operator can support identifying trends, detecting anomalies, and predicting future emissions by scrutinizing the variations in historical data [20]. In Table 1 and Figure 2, we see the most CO_2 emission countries.

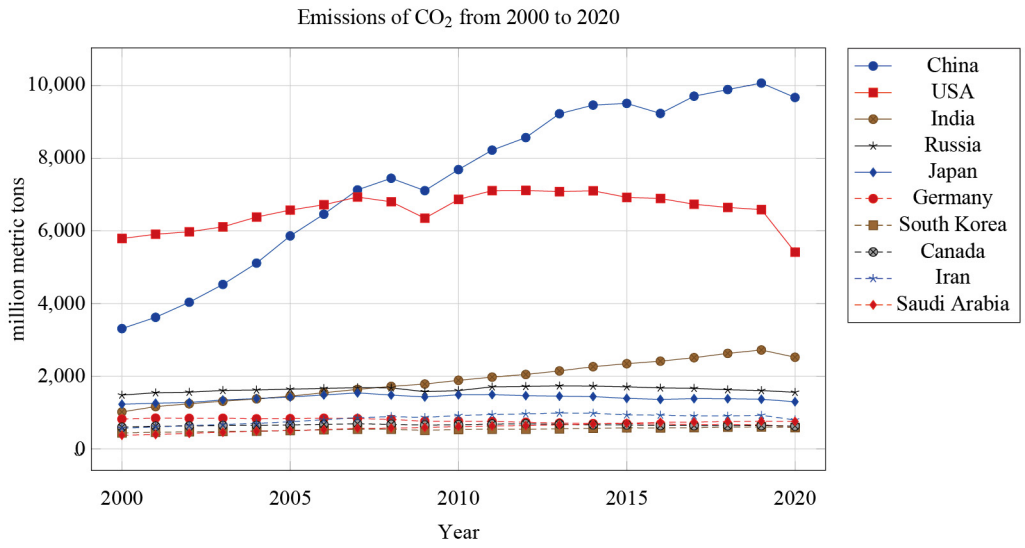


Figure 2. Top 10 countries CO_2 emissions for the year (2000-2020)

This method includes feeding large datasets, such as satellite imagery, industrial output data, and atmospheric measurements, into machine learning algorithms that can then estimate the differences between successive data points [21]. By investigating these differences, AI models can differentiate the rate at which CO_2 levels are rising or falling, contributing insights into the effectiveness of emission reduction schemes and the impact of various human activities on the environment [22]. Furthermore, AI-driven difference operators can increase the accuracy of climate models by refining their input data, foremost to obtain more reliable forecasts. This is particularly important in the fight against climate change, as precise data are crucial for policy-making and international arrangements aimed at reducing the global carbon footprint [23]. Moreover, AI systems can continuously learn and adjust from new data, ensuring that their evaluations remain current and relevant. This adaptability is vital given the dynamic nature of environmental data, where changes can be rapid and complicated. In essence, the integration of AI and difference operators in CO_2 emission and observation studies provides a powerful structure for considering and mitigating the effects of climate change, presenting a level of precision and precaution that traditional approaches struggle to match [24]. This synergy not only develops our ability to observe environmental variations in real-time but also supports the development of proactive measures to address the challenges posed by increasing CO_2 levels [25–27].

Our work organized Figure 3, which is given.

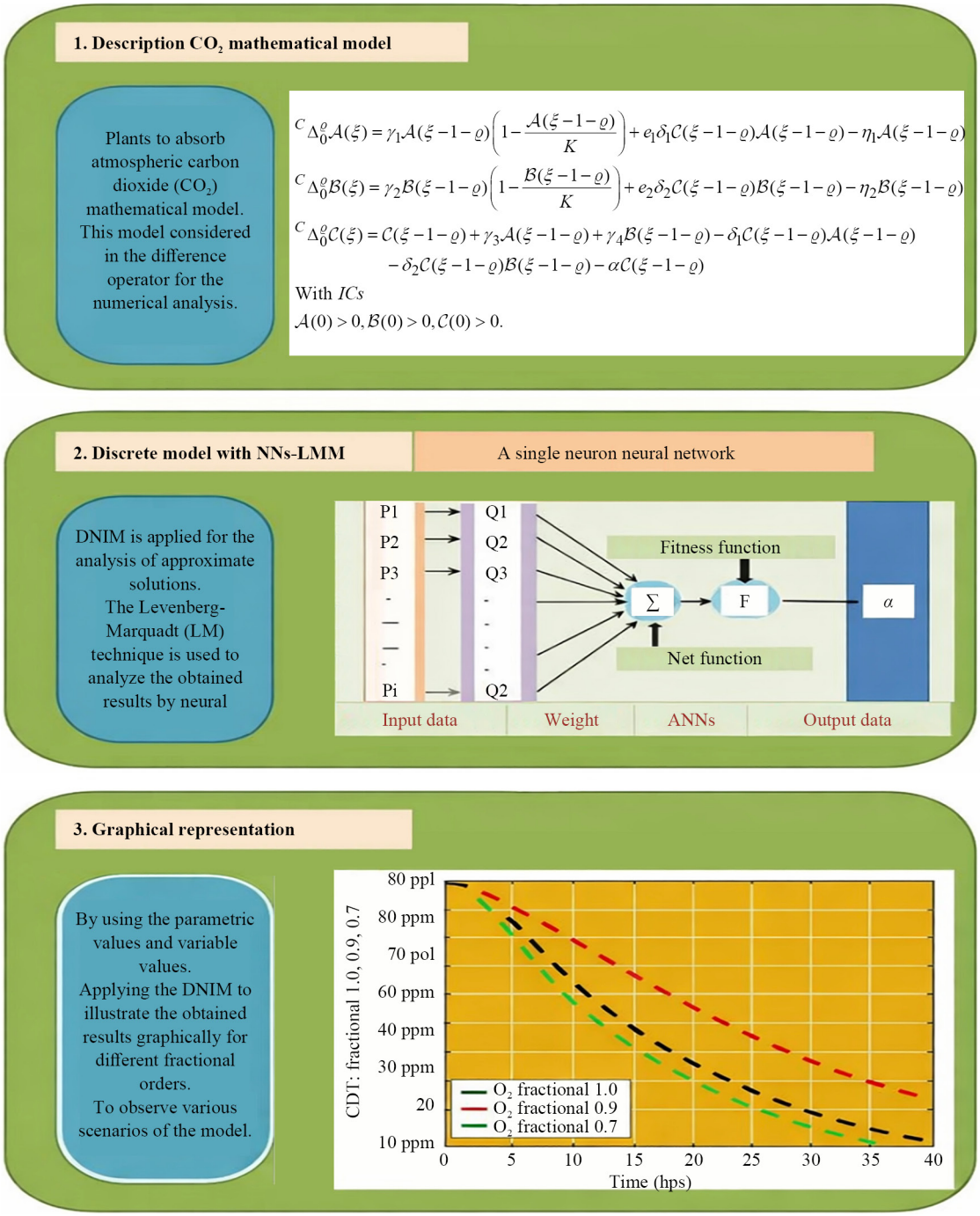


Figure 3. Organization of discrete fraction order plant absorption CO_2

The significance of this study lay in its potential supports to climate changes, and artificial intelligence applications

• Enhanced identifying of CO_2 absorption dynamics: By constructing a mathematical model that replicates how plants absorb carbon dioxide under various conditions, this study can present insights into the proficiency of plants as natural carbon sinker. Visualizing the fractional order discrete models dynamics of plant absorption rates, mainly with different parameters (e.g., absorbing more or less CO_2), can help researchers assess the capacity of plant life to mitigate atmospheric CO_2 levels, an essential factor in global climate variations.

• Application of artificial intelligence for mathematical models: Integrating a neural network, purposely the Levenberg-Marquardt technique, for examining plant-CO_2 interactions brings a novel method to studying complex mathematical processes. AI-based methods allow for accurate regression, fit testing, suitability analysis, and error minimization, delivering more accurate predictions. This can be critical for modeling how ecosystems react to climate change and can guide to better environmental control strategies.

• Impact on discrete fractional calculus in environmental studied: The use of discrete fractional order models provide for more explanation and flexible simulations related to integer-order models. This offers a deeper identification of the long-term memory and hereditary characteristics of plant CO_2 absorption processes. By investigating different fractional orders scenarios, this research opens pathways for upgraded environmental study, especially in identifying non-linear dynamics that manage ecosystem retorts over time.

• Potential contributions to climate change mitigation: With the increasing concentration of atmospheric CO_2 being a serious factor in global warming, identification the role of plants in absorbing CO_2 is essential. This study's findings could inform replanting efforts, agriculture, and land-use planning, offering practical strategies to enhance carbon reduction. By exploring various scenarios through mathematical study and AI-based models, policymakers could construct data-driven decisions for preventing climate change efficiently.

2. Preliminaries results

This section presents the core definitions and key theoretical prospective connected to fractional order sum, and difference orders. For more details the recommended research literature for more exploration, which offers detailed insights and elaborations on these topics. One can found here [28–32].

The Caputo difference operator ${}^{C}\Delta_0^{\rho}\Theta(\xi)$ of a function $\Theta(\xi)$ is formulated as:

$$ {}^{C}\Delta_0^{\rho}\Theta(\xi) = \Delta_0^{-(n-\rho)}\Delta^n\Theta(\xi) = \frac{1}{\Gamma(n-\rho)}\sum_{z=a}^{\xi-(n-\rho)}(\xi-1-z)^{(n-\rho-1)}\Delta^n\Theta(z). \tag{1} $$

Here, $\Delta_0^{-\rho}$ is the fractional order sum, which is given as:

$$ \Delta_0^{-\rho}\Theta(\xi) = \frac{1}{\Gamma(\rho)}\sum_{z=0}^{\xi-\rho}(\xi-1-z)^{(\rho-1)}\Theta(z), \tag{2} $$

with $\rho > 0$. The term $(\xi-1-z)^{(\rho-1)}$ represents the falling function, which is given as:

$$ (\xi-1-z)^{(\rho-1)} = \frac{\Gamma(\xi-z)}{\Gamma(\xi-z-\rho+1)}. $$

3. Model formulation

Mathematical model formulation for plant absorption CO_2 [33–36]. This model is developed in three classes for plant absorption CO_2. Let $\mathscr{A}$ represent the density of plants with a lower capacity for CO_2 absorption, such as herbs and shrubs. Similarly, let $\mathscr{B}$ denote the density of the plants with a higher CO_2 absorption capacity, such as leafy trees. Finally, let $\mathscr{C}$ indicate the concentration of atmospheric CO_2 at any given time t in the region being studied.

$$
\begin{cases}
{}^{C}\Delta_0^{\rho}\mathscr{A}(\xi) = \gamma_1\mathscr{A}(\xi-1-\rho)\left(1-\frac{\mathscr{A}(\xi-1-\rho)}{K}\right)+e_1\delta_1\mathscr{C}(\xi-1-\rho)\mathscr{A}(\xi-1-\rho)-\eta_1\mathscr{A}(\xi-1-\rho)\\
{}^{C}\Delta_0^{\rho}\mathscr{B}(\xi) = \gamma_2\mathscr{B}(\xi-1-\rho)\left(1-\frac{\mathscr{B}(\xi-1-\rho)}{K}\right)+e_2\delta_2\mathscr{C}(\xi-1-\rho)\mathscr{B}(\xi-1-\rho)-\eta_2\mathscr{B}(\xi-1-\rho)\\
{}^{C}\Delta_0^{\rho}\mathscr{C}(\xi) = \mathscr{C}(\xi-1-\rho)+\gamma_3\mathscr{A}(\xi-1-\rho)+\gamma_4\mathscr{B}(\xi-1-\rho)-\delta_1\mathscr{C}(\xi-1-\rho)\mathscr{A}(\xi-1-\rho)\\
\qquad\qquad -\delta_2\mathscr{C}(\xi-1-\rho)\mathscr{B}(\xi-1-\rho)-\alpha\mathscr{C}(\xi-1-\rho)\\
\text{With } ICs\\
\mathscr{A}(0)>0,\ \mathscr{B}(0)>0,\ \mathscr{C}(0)>0.
\end{cases}
\tag{3}
$$

For $\xi \in \mathbb{M}^{1-\rho}$, where $\mathbb{M}^{1-c} = \{c, c+1, c+2, \ldots\}$, $0 < \rho_w \leq 1$, $w = 1, 2, 3$ stand for Caputo difference fractional order operator ${}^{C}\Delta_0^{\rho}\Phi(\xi)$.

The given parameters define the dynamics of two biological entities $\mathscr{A}$ and $\mathscr{B}$ and their interactions with atmospheric CO_2 levels. The intrinsic growth rates of $\mathscr{A}$ and $\mathscr{B}$ are represented by the coefficients γ_1 and γ_2, respectively, measured in units of year^{-1}. The growth rate coefficients of CO_2 due to $\mathscr{A}$ and $\mathscr{B}$ are denoted by γ_3 and γ_4, measured in ppm per ton per year. The carrying capacities for $\mathscr{A}$ and $\mathscr{B}$ are represented by K and L, respectively, in tons. The harvesting rate coefficients for $\mathscr{A}$ and $\mathscr{B}$ are η_1 and η_2, respectively, which are also measured in year^{-1}. Additionally, the uptake rate coefficients of CO_2 by $\mathscr{A}$ and $\mathscr{B}$ are denoted by δ_1 and δ_2, with units of ton^{-1}year^{-1}. The emission rate of CO_2 from natural and anthropogenic sources, excluding the effects of plants, is given by C_1 in ppm per year, whereas the natural depletion rate coefficient of atmospheric CO_2 is represented by α in year^{-1}. Finally, the proportionality constants e_1 and e_2 represent the growth of $\mathscr{A}$ and $\mathscr{B}$ due to CO_2, measured in tons per ppm, with values less than 1. The Figure 4 flow chart of the model 4.

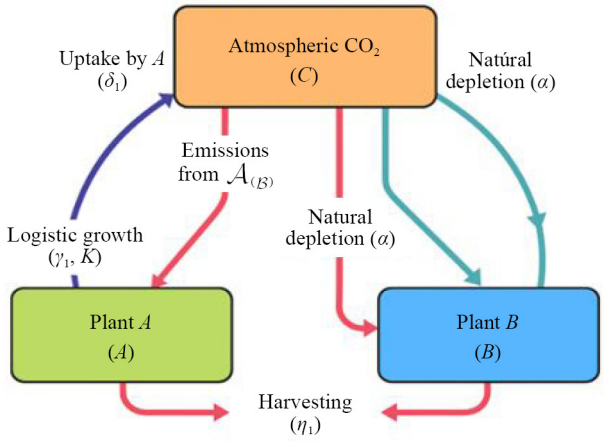


Figure 4. Flow chart of the plant absorption CO_2 model

4. Theoretical analysis of the model

To evaluate the existence of solution and uniqueness of a results for system (3), using fixed point theory together with Picard-Lindelöf theorem. To obtain these results we formulating the system in general form:

$$
\begin{aligned}
&{}^{c}\Delta_{0}^{\rho}\Theta(\xi) = \mathscr{F}(\xi-1+\rho, \Theta(\xi-1+\rho)),\\
&\Theta(0) = \Theta_{0},
\end{aligned}
$$

where $w \in \mathbb{N}_{\max}^{\tau}{}^{1-\rho}$ and $(\tau_{\max}-1+\rho) \in \mathbb{N}$. Here, $\Theta(\xi)$ is defined as $\Theta(\xi) = (\mathscr{A}(\xi), \mathscr{B}(\xi), \mathscr{C}(\xi))^{\tau}$, and the function $\mathscr{F}(\xi, \Theta(\xi))$ is expressed as:

$$
\begin{aligned}
\mathscr{F}_1(\xi, \mathscr{A}) &= \gamma_1\mathscr{A}(\xi)\left(1-\frac{\mathscr{A}(\xi)}{K}\right)+e_1\delta_1\mathscr{C}(\xi)\mathscr{A}(\xi)-\eta_1\mathscr{A}(\xi),\\
\mathscr{F}_2(\xi, \mathscr{B}) &= \gamma_2\mathscr{B}(\xi)\left(1-\frac{\mathscr{B}(\xi)}{K}\right)+e_2\delta_2\mathscr{C}(\xi)\mathscr{B}(\xi)-\eta_2\mathscr{B}(\xi),\\
\mathscr{F}_3(\xi, \mathscr{C}) &= \mathscr{C}(\xi-1-\rho)+\gamma_3\mathscr{A}(\xi-1-\rho)+\gamma_4\mathscr{B}(\xi-1-\rho)\\
&\quad-\delta_1\mathscr{C}(\xi-1-\rho)\mathscr{A}(\xi-1-\rho)-\delta_2\mathscr{C}(\xi-1-\rho)\mathscr{B}(\xi-1-\rho)-\alpha\mathscr{C}(\xi-1-\rho).
\end{aligned}
\tag{4}
$$

To extend the study of existence of results and uniqueness of solution, we use the initial condition $\Theta(0)$ and leveraging Proposition 1. Through this technique, system (3) is reformulating into a gathering of summation equations. We have

$$
\begin{aligned}
\mathscr{A}(\xi)-\mathscr{A}(0) &= \Delta_{1-\rho}^{-\rho}\left(\gamma_1\mathscr{A}(\xi-1-\rho)\left(1-\frac{\mathscr{A}(\xi-1-\rho)}{K}\right)+e_1\delta_1\mathscr{C}(\xi-1-\rho)\mathscr{A}(\xi-1-\rho)-\eta_1\mathscr{A}(\xi-1-\rho)\right),\\
\mathscr{B}(\xi)-\mathscr{B}(0) &= \Delta_{1-\rho}^{-\rho}\left(\gamma_2\mathscr{B}(\xi-1-\rho)\left(1-\frac{\mathscr{B}(\xi-1-\rho)}{K}\right)+e_2\delta_2\mathscr{C}(\xi-1-\rho)\mathscr{B}(\xi-1-\rho)-\eta_2\mathscr{B}(\xi-1-\rho)\right),\\
\mathscr{C}(\xi)-\mathscr{C}(0) &= \Delta_{1-\rho}^{-\rho}\left(\mathscr{C}(\xi-1-\rho)+\gamma_3\mathscr{A}(\xi-1-\rho)+\gamma_4\mathscr{B}(\xi-1-\rho)\right.\\
&\quad\left.-\delta_1\mathscr{C}(\xi-1-\rho)\mathscr{A}(\xi-1-\rho)-\delta_2\mathscr{C}(\xi-1-\rho)\mathscr{B}(\xi-1-\rho)-\alpha\mathscr{C}(\xi-1-\rho)\right),
\end{aligned}
$$

for $w \in \mathbb{M}^{\tau_{\max}1-\rho}$. With the aid of the given system alongside Definition 1, we can develop the illustration of the state variables consequently $\mathscr{A}(\xi)$, $\mathscr{B}(\xi)$, and $\mathscr{C}(\xi)$ in terms of $\mathscr{F}_i(\xi, \Theta(\xi))$, where $i = 1, 2, 3$. Specifically, we have:

$$\mathscr{A}(\xi)-\mathscr{A}(0)=\Delta_{1-\rho}^{-\rho}\left[\gamma_1\mathscr{A}(\xi-1-\rho)\left(1-\frac{\mathscr{A}(\xi-1-\rho)}{K}\right)\right.$$

$$\left.+e_1\delta_1\mathscr{C}(\xi-1-\rho)\mathscr{A}(\xi-1-\rho)-\eta_1\mathscr{A}(\xi-1-\rho)\right],$$

$$\mathscr{B}(\xi)-\mathscr{B}(0)=\Delta_{1-\rho}^{-\rho}\left[\gamma_2\mathscr{B}(\xi-1-\rho)\left(1-\frac{\mathscr{B}(\xi-1-\rho)}{K}\right)\right.$$

$$\left.+e_2\delta_2\mathscr{C}(\xi-1-\rho)\mathscr{B}(\xi-1-\rho)-\eta_2\mathscr{B}(\xi-1-\rho)\right], \tag{5}$$

$$\mathscr{C}(\xi)-\mathscr{C}(0)=\Delta_{1-\rho}^{-\rho}\left[\mathscr{C}(\xi-1-\rho)+\gamma_3\mathscr{A}(\xi-1-\rho)+\gamma_4\mathscr{B}(\xi-1-\rho)\right.$$

$$\left.-\delta_1\mathscr{C}(\xi-1-\rho)\mathscr{A}(\xi-1-\rho)-\delta_2\mathscr{C}(\xi-1-\rho)\mathscr{B}(\xi-1-\rho)-\alpha\mathscr{C}(\xi-1-\rho)\right].$$

for $w\in\mathbb{M}_{1-\rho}^{\tau_{\max}}$.

By levering Picard iterations, we can formulate the following recursive system:

$$\mathscr{A}_{n+1}(\xi)=\mathscr{A}(0)+\frac{1}{\Gamma(\rho)}\sum_{s=1-\rho}^{w-\rho}(\xi-s-1)^{\rho-1}\mathscr{F}_1(s-1+\rho,\mathscr{A}_n(s-1+\rho)),$$

$$\mathscr{B}_{n+1}(\xi)=\mathscr{B}(0)+\frac{1}{\Gamma(\rho)}\sum_{s=1-\rho}^{w-\rho}(\xi-s-1)^{\rho-1}\mathscr{F}_2(s-1+\rho,\mathscr{B}_n(s-1+\rho)),$$

$$\mathscr{C}_{n+1}(\xi)=\mathscr{C}(0)+\frac{1}{\Gamma(\rho)}\sum_{s=1-\rho}^{w-\rho}(\xi-s-1)^{\rho-1}\mathscr{F}_3(s-1+\rho,\mathscr{C}_n(s-1+\rho)),$$

for $w\in\mathbb{M}_{1-\rho}^{\tau_{\max}}$.

Considering the iterative framework and using the initial condition, we deduce the below sum equation:

$$\Theta(\xi)=\Theta(0)+\frac{1}{\Gamma(\rho)}\sum_{s=1-\rho}^{w-\rho}(\xi-s-1)^{\rho-1}\mathscr{F}(s-1+\rho,\Theta(s-1+\rho)),$$

where $w\in\mathbb{M}_1$.

From this investigation, we establish theoretical solutions that verify the existence and uniqueness of a results for the system. Here's rearranging the lemma, proof, and related inequalities as given.

Lemma 1 The $\mathscr{F}(\xi, \Theta(\xi))$ function given in the equation (4), satisfies the Lipschitz criterion:

$$\|\mathscr{F}(\xi, \Theta(\xi)) - \mathscr{F}(\xi, \Theta'(\xi))\| \leq b\|\Theta(\xi) - \Theta'(\xi)\|, \tag{6}$$

where

$$b = \max\Big\{\max\|\gamma_1\left(1 - \frac{\mathscr{A}(\xi)}{K}\right) + e_1\delta_1\mathscr{C}(\xi) - \eta_1\|, \max\|(\gamma_2\left(1 - \frac{\mathscr{B}(\xi)}{K}\right) + e_2\delta_2\mathscr{C}(\xi) - \eta_2)\|,$$

$$\|(\gamma_4\mathscr{B}(\xi) + (1 + \gamma_3 - \delta_1)\mathscr{A}(\xi))\|\Big\}.$$

Proof. Consider $\mathscr{A}$ and $\mathscr{A}'(\xi)$ two functions, such that:

$$\|\mathscr{F}_1(\xi, \mathscr{A}) - \mathscr{F}_1(\xi, \mathscr{A}')\| = \|(\gamma_1\left(1 - \frac{\mathscr{A}(\xi)}{K}\right) + e_1\delta_1\mathscr{C}(\xi) - \eta_1)(\mathscr{A} - \mathscr{A}')\|.$$

Further, taking into account that:

$$b_1 = \max\|(\gamma_1\left(1 - \frac{\mathscr{A}(\xi)}{K}\right) + e_1\delta_1\mathscr{C}(\xi) - \eta_1)\|,$$

we obtain:

$$\|\mathscr{F}_1(\xi, \mathscr{A}) - \mathscr{F}_1(\xi, \mathscr{A}')\| \leq b_1\|\mathscr{A} - \mathscr{A}'\|.$$

Following similar reasoning, we obtain the following inequalities:

$$\|\mathscr{F}_2(\xi, \mathscr{B}) - \mathscr{F}_2(\xi, \mathscr{B}')\| \leq b_2\|\mathscr{B} - \mathscr{B}'\|, \quad \|\mathscr{F}_3(\xi, \mathscr{C}) - \mathscr{F}_3(\xi, \mathscr{C}')\| \leq b_3\|\mathscr{C} - \mathscr{C}'\|,$$

where

$$b_2 = \max\|(\gamma_2\left(1 - \frac{\mathscr{B}(\xi)}{K}\right) + e_2\delta_2\mathscr{C}(\xi) - \eta_2)\|, \quad b_3 = \|(\gamma_4\mathscr{B}(\xi) + (1 + \gamma_3 - \delta_1)\mathscr{A}(\xi))\|.$$

This followed that the functions $\mathscr{F}_1$, $\mathscr{F}_2$, and $\mathscr{F}_3$ confirms the Lipschitz property. Moreover, if $b_z < 1$, then the considered function $\mathscr{F}_z$ fulfill contraction property for $z = 1, 2, 3$. □

Theorem 1 Let the condition (6) is satisfied. Then, this guarantees a unique solution of the considered system (3) if

$$\frac{(\tau_{\max}-1+\rho)}{\Gamma(\rho+1)}b<1.$$

Proof. We can express the solution system (3) as follow:

$$\Theta(\xi)=\mathscr{W}(\Theta(\xi)),$$

where $\mathscr{W}$ is the Picard technique is given as:

$$\mathscr{W}(\Theta(\xi))=\Theta(0)+\frac{1}{\Gamma(\rho)}\sum_{z=1}^{w-\rho}(\xi-z-1)^{\rho-1}\mathscr{F}(z-1+\rho,\Theta(z-1+\rho)).$$

By following the arguments, we get:

$$\|\mathscr{W}(\Theta_1(\xi))-\mathscr{W}(\Theta_2(\xi))\|=\frac{1}{\Gamma(\rho)}\sum_{z=1}^{w-\rho}(\xi-z-1)^{\rho-1}\|\mathscr{F}(z-1+\rho,\Theta_1(z-1+\rho))-\mathscr{F}(z-1+\rho,\Theta_2(z-1+\rho))\|.$$

Thus, we have:

$$\|\mathscr{W}(\Theta_1(\xi))-\mathscr{W}(\Theta_2(\xi))\|\leq\frac{1}{\Gamma(\rho)}\sum_{z=1}^{w-\rho}(\xi-z-1)^{\rho-1}\|\mathscr{F}(z-1+\rho,\Theta_1(z-1+\rho))-\mathscr{F}(z-1+\rho,\Theta_2(z-1+\rho))\|,$$

which simplifies further to:

$$\|\mathscr{W}(\Theta_1(\xi))-\mathscr{W}(\Theta_2(\xi))\|\ \leq\frac{1}{\Gamma(\rho)}\left(\sum_{z=1}^{w-\rho}(\xi-z-1)^{\rho-1}\right)\max_{z\in\mathbb{N}}\|\mathscr{F}(z-1+\rho,\Theta_1(z-1+\rho))-$$

$$\mathscr{F}(z-1+\rho,\Theta_2(z-1+\rho))\|,$$

leading to:

$$\|\mathscr{W}(\Theta_1(\xi))-\mathscr{W}(\Theta_2(\xi))\|\leq\frac{(\xi-1+\rho)}{\Gamma(\rho+1)}b\|\Theta_1(\xi)-\Theta_2(\xi)\|.$$

Since

$$\frac{(\tau_{\max}-1+\rho)}{\Gamma(\rho+1)}b<1.$$

Where, $\mathscr{W}$ fulfill contraction property for $\xi \leq \tau_{\max}$. Therefore, system (3), has a unique solution. □

5. Numerical simulations

The discrete fractional order plant absorbs the CO_2 model, which includes the Caputo operator, and is subject to an iterative numerical analysis via first-order discrete numerical methods as explained in [37, 38]. These techniques are well-regarded for their high degree of accuracy and their reliable properties. They also exhibit conditional stability, making them suitable for application to both linear and fractional-order nonlinear models. By employing these methods, the study aims to guarantee that the numerical results are both precise and stable, regardless of the complexity of the fractional order discrete model under consideration.

Consider the following delta difference frcational order system:

$$ {}^{C}\Delta_a^{\rho_i}\Theta(\xi) = g(\xi+\rho_i-1, y(\xi+\rho_i-1)), \tag{7} $$

$$ \Theta(0) = \Theta_0. \tag{8} $$

By utilizing $\Delta_0^{-\rho}$ to both side of Eq. (8), we obtain unique solution problem (3) is gives:

$$ \Theta(\xi) = \Theta_0(\xi) + \frac{1}{\Gamma(\rho_i)} \sum_{\tau=a+z-\rho_i}^{r-\rho_i} (\xi-\sigma(\tau))^{\rho_i-1} g(\tau+\rho_i-1, \Theta(\tau+\rho_i-1)), \quad w \in M_{w+z}, \tag{9} $$

where

$$ \Theta_0(\xi) = \sum_{\rho=0}^{z-1} \frac{(\xi-a)^{\rho}}{\Gamma(\rho+1)} \Delta^{\rho}\Theta(a). \tag{10} $$

Where, $\Theta = (p_1, p_2, p_3) \in \mathscr{R}_+^3$ denotes a continuous function. By operating the $\Delta_0^{-\rho}$ sum operator. We divide the interval $[0, \tau]$ into equally spaced segments with a constant step size k, where $k = \tau z$ and $z \in \mathbb{M}$. This method allows us to approximate the value of $\Theta(\xi)$ at time points $t = t_j$, for $j = 0, 1, \ldots, p$. Let

$$ \begin{cases} \Omega_1 = \gamma_1 \mathscr{A}(\xi-1-\rho)\left(1-\dfrac{\mathscr{A}(\xi-1-\rho)}{K}\right) + e_1\delta_1\mathscr{C}(\xi-1-\rho)\mathscr{A}(\xi-1-\rho) - \eta_1\mathscr{A}(\xi-1-\rho), \\ \Omega_2 = \gamma_2 \mathscr{B}(\xi-1-\rho)\left(1-\dfrac{\mathscr{B}(\xi-1-\rho)}{K}\right) + e_2\delta_2\mathscr{C}(\xi-1-\rho)\mathscr{B}(\xi-1-\rho) - \eta_2\mathscr{B}(\xi-1-\rho), \\ \Omega_3 = \mathscr{C}(\xi-1-\rho) + \gamma_3\mathscr{A}(\xi-1-\rho) + \gamma_4\mathscr{B}(\xi-1-\rho) - \delta_1\mathscr{C}(\xi-1-\rho)\mathscr{A}(\xi-1-\rho) \\ \qquad -\delta_2\mathscr{C}(\xi-1-\rho)\mathscr{B}(\xi-1-\rho) - \alpha\mathscr{C}(\xi-1-\rho). \end{cases} \tag{11} $$

The iterative numerical method constructed for the considered model in the sense of Caputo operator:

$$\mathscr{A}(\xi) = \mathscr{A}(0) + \frac{1}{\Gamma(\rho)} \sum_{j=0}^{\xi-1} \frac{\Gamma(\xi - j - 1 + \rho)}{\Gamma(\xi - j)} \Omega_1(j),$$

$$\mathscr{B}(\xi) = \mathscr{B}(0) + \frac{1}{\Gamma(\rho)} \sum_{j=0}^{\xi-1} \frac{\Gamma(\xi - j - 1 + \rho)}{\Gamma(\xi - j)} \Omega_2(j), \tag{12}$$

$$\mathscr{C}(\xi) = \mathscr{C}(0) + \frac{1}{\Gamma(\rho)} \sum_{j=0}^{\xi-1} \frac{\Gamma(\xi - j - 1 + \rho)}{\Gamma(\xi - j)} \Omega_3(j).$$

We focus on investigating the differences between iterative terms in the sequences, for each difference is calculated by fractional order power terms. This finding helps with the discrete structure of fractional calculus, fpr summation is used in place of integration, and finite differences attend as substitutes for differential operators. We now turn our attention to the numerical outcomes associated with the model's approximate results. For this purpose, Euler method was utilized in the connection of Caputo fractional operator.

6. Neural network analysis of discrete model

The study of how plants capture CO_2 has focused on a new dimension with the application of neural networking procedures, leading to more meticulous and nuanced visions of this critical procedure. For the neural network analysis one can see, [39–48]. Plants play a basic role in the carbon cycle, performing as major decline for atmospheric CO_2 through photosynthesis, where CO_2 is improved into organic matter, fueling plant growth and facilitating the regulation of global carbon levels.

However, the efficiency and capacity of plants to absorb CO_2 can vary extensively on the basis of several factors, including species, environmental conditions, soil quality, and even the age of the plant. Traditional approaches for studying this absorption process have provided valuable data, but they often fail to capture the full complexity and variability of real-world conditions. This is where neural networking is an effective tool that can investigate vast amounts of data and uncover forms that might be invisible through conventional examination. The neural network structure is designed in the Figure 5, input, hidden layer, output layer and output.

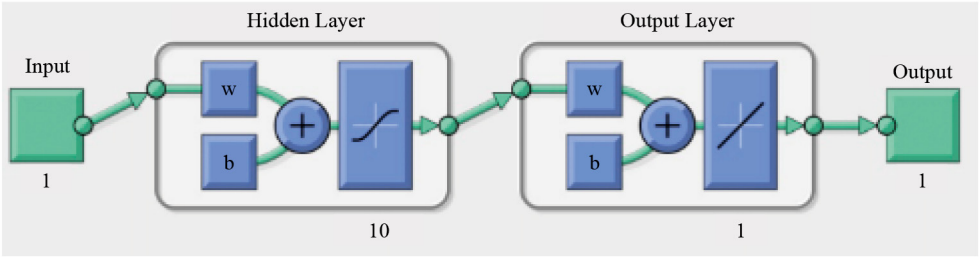


Figure 5. Neural network framework of the system (3), model

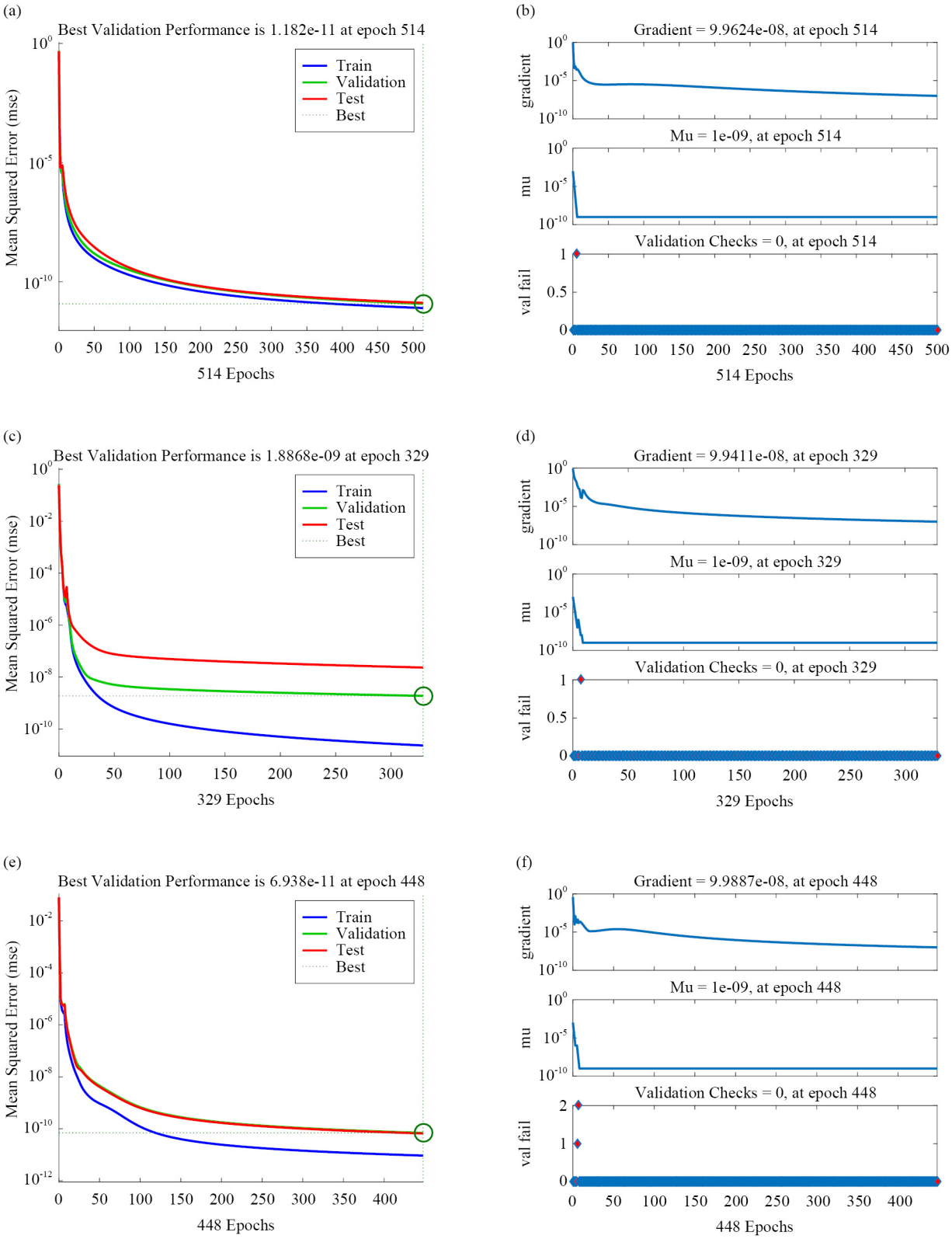


Figure 6. Different fractional order cases of MSE and training test demonstrate the considered model (3). (a) For Case 1: On epochs 514 MSE performance of the model (13); (b) For Case 1: On epochs 514 training test of the model (13); (c) For Case 2: On epochs 329 MSE performance of the model (14); (d) For Case 2: On epochs 329 training test for of the model (14); (e) For Case 3: On epochs 448 MSE performance for epochs 81 of the model (15); (f) For Case 3: On epochs 448 training test of the model (15)

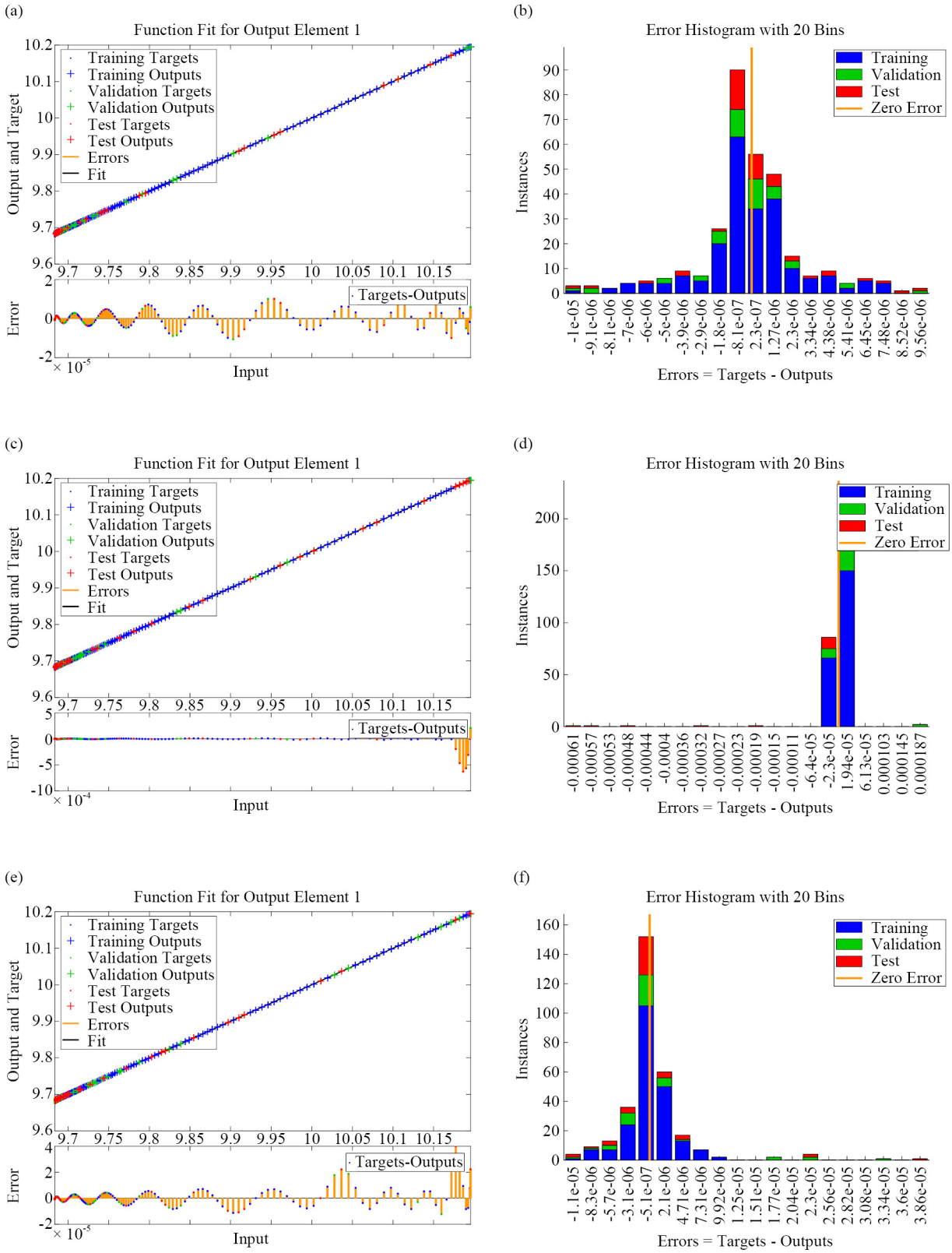
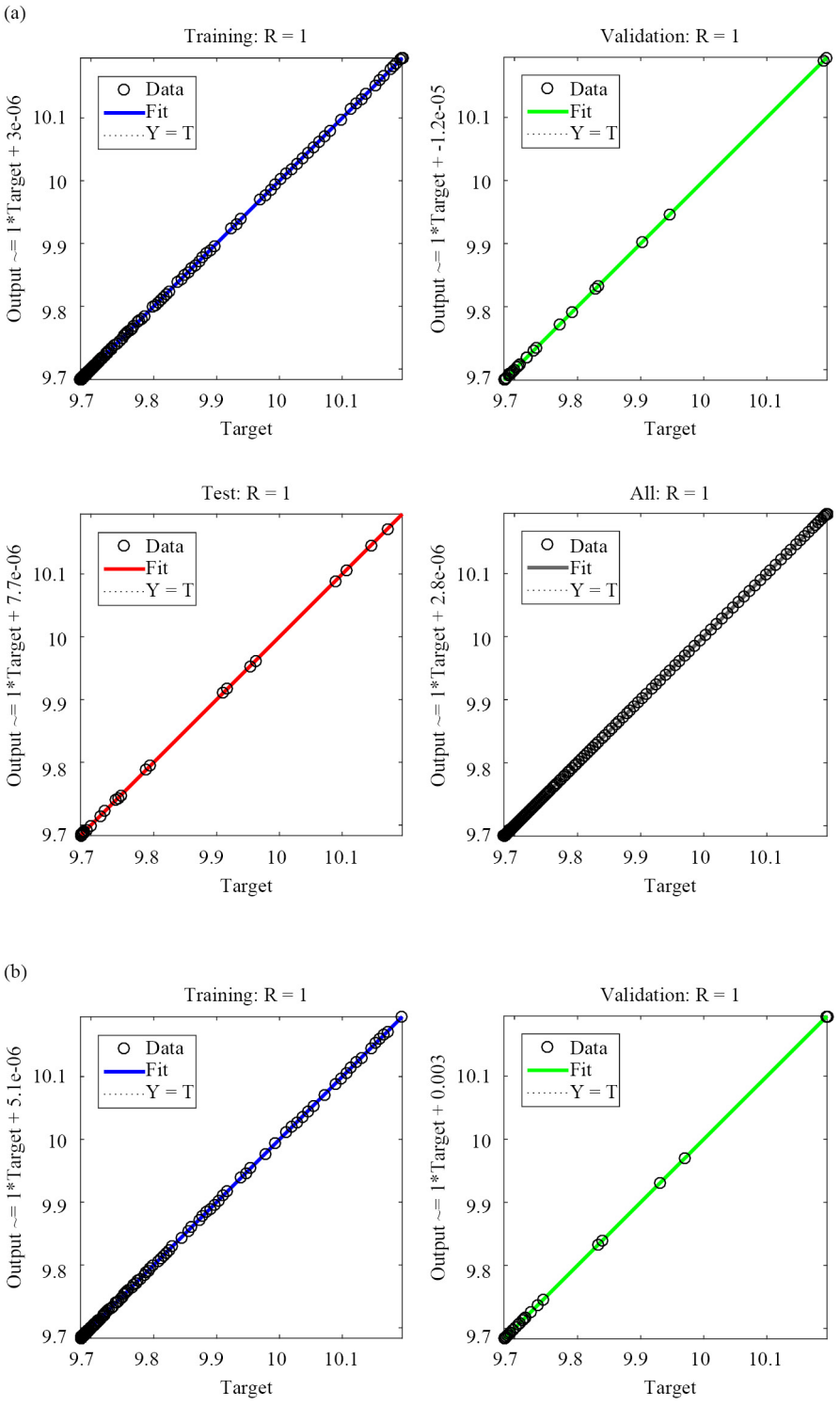


Figure 7. Three different cases of the discrete fractional order model (3). (a) For Case 1: On epoch 514 training fit of the model (13); (b) For Case 1: On epoch 514 training histogram of the model (13); (c) For Case 2: On epochs 329 training fit of the model (14); (d) For Case 2: On epochs 329 training histogram of the model (14); (e) For Case 3: On epochs 448 training fit of the model (15); (f) For Case 3: On epochs 448 training histogram of the model (15)


(a)
Training: R = 1
Validation: R = 1
Test: R = 1
All: R = 1
Data
Fit
Y = T
Output ~= 1*Target + 3e-06
Output ~= 1*Target + -1.2e-05
Output ~= 1*Target + 7.7e-06
Output ~= 1*Target + 2.8e-06
Target
9.7
9.8
9.9
10
10.1
(b)
Training: R = 1
Validation: R = 1
Output ~= 1*Target + 5.1e-06
Output ~= 1*Target + 0.003

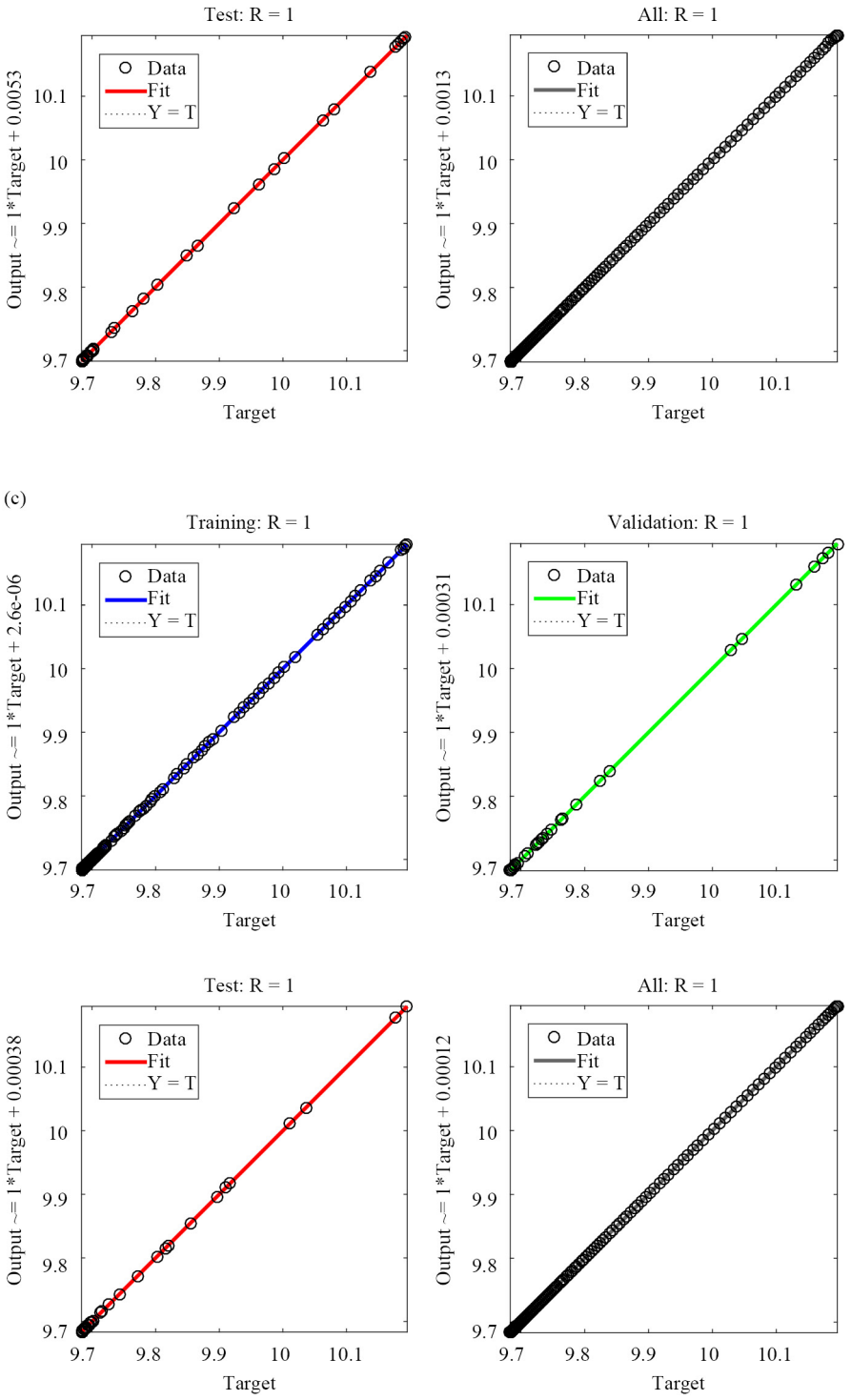


Figure 8. Three different cases for the training regression of the model (3). (a) For Case 1: On epochs 514 training regression of the model (13); (b) For Case 2: One epochs 329 training regression of the model (14); (c) For Case 3: On epochs 448 training regression of the model (15)

In Figure 6, we examine Mean Squared Errors (MSEs) and training tests for three cases such that: Case 1, Case 2, and Case 3 for various fractional orders of the discrete fractional order plant absorb CO_2 (3). In Figure 7, we study training fit and training histogram for three cases such as: Case 1, Case 2, and Case 3 by using fractional orders of the discrete model

(3). In Figure 8, we check training regression for three cases for various orders of the discrete model (3) The performance with neural networking is calculated by many metrics, including regression analysis, mean squared error, and fit assessment. We visualize the error histograms and distribution of prediction errors, highlighting the model's accuracy. Regression studies gives vision of the correlation among predicted and real solutions, whereas training and model fit provided a broad assessment of the neural network's technique. The important benefit of the use of neural networks in this frame is their skill to grip nonlinearities and difficult connections inside the data, are usual in discrete models. The neural network's approach overcomes such complexities, with multiple layers and an iterative numerical algorithm tailored to optimize performance. In addition, the regularization technique checks overfitting, ensuring that the model generalizes well and accurately.

7. Numerical discussion

We investigate the discrete fractional order plant absorb CO_2 model within the context of Caputo operator to demonstrate its dynamics. Iterative numerical method formulated to get approximate solutions of the considered model. The results, as illustrated in the referenced figure, show that the fractional order dynamics closely behave those of an integer order, considering a strong correlation. By fixing the variable class and parametric values, we identified valuable outlines in the considered model's dynamics. The analysis specifically absorbed on three cases of fractional orders one can see Figures 9–11, each showing unique characteristics of the suggested model's dynamics. This method provided a deeper identifying of how fractional calculus can value to the discrete considered model, present insights that could be applicable in future studies.

Case 1 For the fractional order $\rho_1 = 0.9, 0.7, 0.5$, of the class $\mathscr{A}$, of the discrete fractional order plant absorb CO_2 model. Faxing the parametric values of the considered model. such, $e1 = 0.05$, $e2 = 0.06$, $\gamma_1 = 0.1$, $\gamma_2 = 0.2$, $\gamma_3 = 0.001$, $\gamma_4 = 0.002$, $\eta_1 = 0.06$, $\eta_2 = 0.02$, $K = 2,000$, $L = 1,000$, $c1 = 1$, $\delta_1 = 0.0001$, $\delta_2 = 0.0003$, $\alpha = 0.003$. and with variable initial values ($\mathscr{A} = 801.0195$, $\mathscr{B} = 900.9176$, $\mathscr{C} = 10.1955$).

$$
\begin{cases}
{}^{C}\Delta_0^{\rho_1}\mathscr{A}(\xi) = \gamma_1\mathscr{A}(\xi-1-\rho_1)\left(1-\frac{\mathscr{A}(\xi-1-\rho_1)}{K}\right)+e_1\delta_1\mathscr{C}(\xi-1-\rho_1)\mathscr{A}(\xi-1-\rho_1)-\eta_1\mathscr{A}(\xi-1-\rho_1) \\
{}^{C}\Delta_0^{\rho_1}\mathscr{B}(\xi) = \gamma_2\mathscr{B}(\xi-1-\rho_1)\left(1-\frac{\mathscr{B}(\xi-1-\rho_1)}{K}\right)+e_2\delta_2\mathscr{C}(\xi-1-\rho_1)\mathscr{B}(\xi-1-\rho_1)-\eta_2\mathscr{B}(\xi-1-\rho_1) \\
{}^{C}\Delta_0^{\rho_1}\mathscr{C}(\xi) = \mathscr{C}(\xi-1-\rho_1)+\gamma_3\mathscr{A}(\xi-1-\rho_1)+\gamma_4\mathscr{B}(\xi-1-\rho_1)-\delta_1\mathscr{C}(\xi-1-\rho_1)\mathscr{A}(\xi-1-\rho_1) \\
\qquad\qquad -\delta_2\mathscr{C}(\xi-1-\rho_1)\mathscr{B}(\xi-1-\rho_1)-\alpha\mathscr{C}(\xi-1-\rho_1).
\end{cases}
\tag{13}
$$

Case 2 For the fractional order $\rho_2 = 0.9, 0.7, 0.5$, of the class $\mathscr{B}$, of the discrete fractional order plant absorb CO_2 model. Faxing the parametric values of the considered model. such, $e1 = 0.05$, $e2 = 0.06$, $\gamma_1 = 0.1$, $\gamma_2 = 0.2$, $\gamma_3 = 0.001$, $\gamma_4 = 0.002$, $\eta_1 = 0.06$, $\eta_2 = 0.02$, $K = 2,000$, $L = 1,000$, $c1 = 1$, $\delta_1 = 0.0001$, $\delta_2 = 0.0003$, $\alpha = 0.003$. and with variable initial values ($\mathscr{A} = 801.0195$, $\mathscr{B} = 900.9176$, $\mathscr{C} = 10.1955$).

$$
\begin{cases}
{}^{C}\Delta_0^{\rho_2}\mathscr{A}(\xi) = \gamma_1\mathscr{A}(\xi-1-\rho_2)\left(1-\frac{\mathscr{A}(\xi-1-\rho_2)}{K}\right)+e_1\delta_1\mathscr{C}(\xi-1-\rho_2)\mathscr{A}(\xi-1-\rho_2)-\eta_1\mathscr{A}(\xi-1-\rho_2)\\
{}^{C}\Delta_0^{\rho_2}\mathscr{B}(\xi) = \gamma_2\mathscr{B}(\xi-1-\rho_2)\left(1-\frac{\mathscr{B}(\xi-1-\rho_2)}{K}\right)+e_2\delta_2\mathscr{C}(\xi-1-\rho_2)\mathscr{B}(\xi-1-\rho_2)-\eta_2\mathscr{B}(\xi-1-\rho_2)\\
{}^{C}\Delta_0^{\rho_2}\mathscr{C}(\xi) = \mathscr{C}(\xi-1-\rho_2)+\gamma_3\mathscr{A}(\xi-1-\rho_2)+\gamma_4\mathscr{B}(\xi-1-\rho_2)-\delta_1\mathscr{C}(\xi-1-\rho_2)\mathscr{A}(\xi-1-\rho_2)\\
\qquad\qquad -\delta_2\mathscr{C}(\xi-1-\rho_2)\mathscr{B}(\xi-1-\rho_2)-\alpha\mathscr{C}(\xi-1-\rho_2).
\end{cases}
\tag{14}
$$

Case 3 For the fractional order $\rho_3 = 0.9, 0.7, 0.5$, of the class $\mathscr{C}$, of the discrete fractional order plant absorb CO_2 model. Faxing the parametric values of the considered model. such, $e1 = 0.05$, $e2 = 0.06$, $\gamma_1 = 0.1$, $\gamma_2 = 0.2$, $\gamma_3 = 0.001$, $\gamma_4 = 0.002$, $\eta_1 = 0.06$, $\eta_2 = 0.02$, $K = 2,000$, $L = 1,000$, $c1 = 1$, $\delta_1 = 0.0001$, $\delta_2 = 0.0003$, $\alpha = 0.003$. and with variable initial values ($\mathscr{A} = 801.0195$, $\mathscr{B} = 900.9176$, $\mathscr{C} = 10.1955$).

$$
\begin{cases}
{}^{C}\Delta_0^{\rho_3}\mathscr{A}(\xi) = \gamma_1\mathscr{A}(\xi-1-\rho_3)\left(1-\frac{\mathscr{A}(\xi-1-\rho_3)}{K}\right)+e_1\delta_1\mathscr{C}(\xi-1-\rho_3)\mathscr{A}(\xi-1-\rho_3)-\eta_1\mathscr{A}(\xi-1-\rho_3)\\
{}^{C}\Delta_0^{\rho_3}\mathscr{B}(\xi) = \gamma_2\mathscr{B}(\xi-1-\rho_3)\left(1-\frac{\mathscr{B}(\xi-1-\rho_3)}{K}\right)+e_2\delta_2\mathscr{C}(\xi-1-\rho_3)\mathscr{B}(\xi-1-\rho_3)-\eta_2\mathscr{B}(\xi-1-\rho_3)\\
{}^{C}\Delta_0^{\rho_3}\mathscr{C}(\xi) = \mathscr{C}(\xi-1-\rho_3)+\gamma_3\mathscr{A}(\xi-1-\rho_3)+\gamma_4\mathscr{B}(\xi-1-\rho_3)-\delta_1\mathscr{C}(\xi-1-\rho_3)\mathscr{A}(\xi-1-\rho_3)\\
\qquad\qquad -\delta_2\mathscr{C}(\xi-1-\rho_3)\mathscr{B}(\xi-1-\rho_3)-\alpha\mathscr{C}(\xi-1-\rho_3).
\end{cases}
\tag{15}
$$

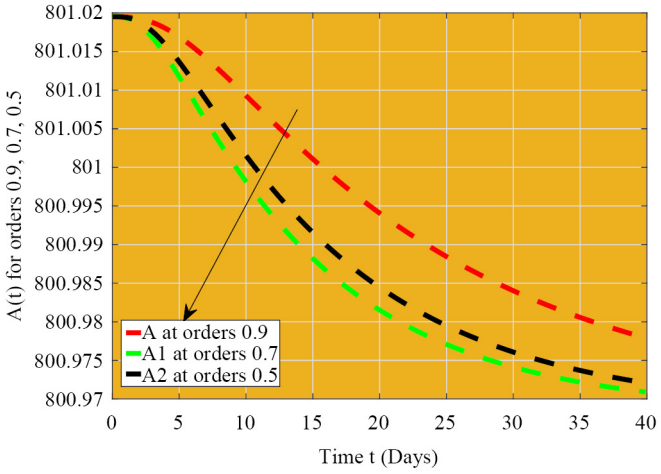


Figure 9. Time series of the class $\mathscr{A}$ of the system (3) for the fractional order values of $\rho_1 = 0.9, 0.7, 0.5$

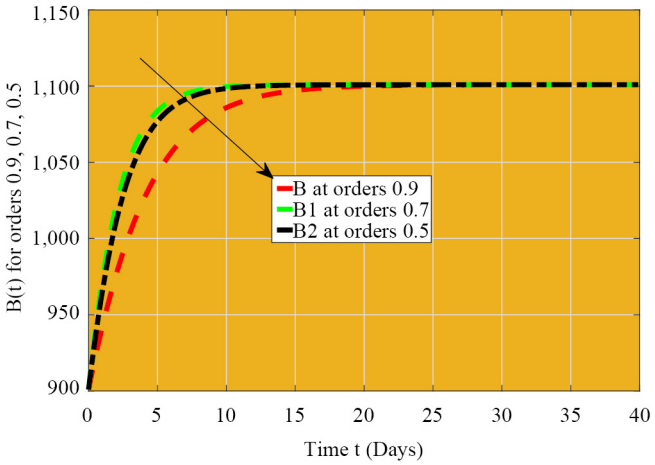


Figure 10. Time series of the class $\mathscr{B}$ of the system (3) for the fractional order values of $\rho_1 = 0.9, 0.7, 0.5$

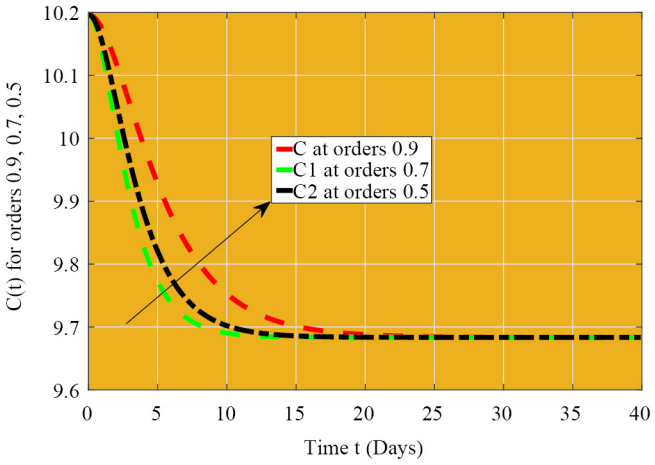


Figure 11. Time series of the class $\mathscr{C}$ of the system (3) for the fractional order values of $\rho_1 = 0.9, 0.7, 0.5$

8. Conclusion

This work focuses on a fractional order discrete mathematical model that simulates the capture of CO_2 by plants. The study explain a rapid approximation method employing the Caputo fractional order to examine the model under different fractional orders. The outcomes of the study are evaluated by comparing for fractional orders to reveal their effectiveness in the discrete fractional-order plant CO_2 absorption model. Assessment metrics contain error histograms, fit evaluations, regression analysis, and training performance of the considered model. For statistical analysis, the dataset was distributed into two subsets: 70% for training, 15% for authentication, and 15% for testing. Figures 6–8 elucidate various aspects of the model's performance across various fractional orders. In particular, Figure 6 explain the Mean Squared Errors (MSEs) and training tests for three cases across fractional orders, while Figure 7 gives details on training fit and histograms. Figure 8 explores training regression for the same cases and fractional orders. This dataset split validates a rigorous assessment of the three considered model's predictive proficiencies. Future outlines in this area could contain investigation of other fractional derivative and operating the model to more complex datasets to verify and develop its performance. Moreover, researchers might explore the effect of different training status splits to classify the optimal ratio for various datasets. Expanding the considered model to handle multidimensional data might also offer greater comprehensions into its real-world applicability. Another encouraging research direction is the improvement of hybrid models that connect the

Caputo operator with other several numerical procedures to boost accuracy and proficiency. By pursuing these research paths, future studies can construct on the initial work accessible here, advancing the empathetic and concentration of fractional order discrete models in plant CO_2 absorption studies. This work has the potential to give significantly to the early detection of such type mathematical models, delivered the models are further refined and confirmed in subsequent studies.

Acknowledgement

Aziz Khan and Thabet Abdeljawad would like to thank Prince Sultan University for paying the APC and for the support through TAS research lab.

Contributions

Aziz Khan: Writing–original draft, Conceptualization. Hadeel Bin Amer: Formal analysis. Thabet Abdeljawad: Investigation. Rajermani Thinakaran: Supervision.

Data availability

All data available inside the manuscript.

Conflict of interest

The authors declare no competing financial interest.

References

[1] Dervash MA, Yousuf A, Ozturk M, Bhat RA. Global warming: impacts of temperature escalation. In: *Phytosequestration: Strategies for Mitigation of Aerial Carbon Dioxide and Aquatic Nutrient Pollution*. Springer International Publishing; 2023. p.27–36.

[2] Roebroek CT, Duveiller G, Seneviratne SI, Davin EL, Cescatti A. Releasing global forests from human management: how much more carbon could be stored? *Science*. 2023; 380(6646): 749–753. Available from: https://doi.org/10.1126/science.add5878.

[3] Sultan U, Zhang Y, Farooq M, Imran M, Khan AA, Zhuge W, et al. Qualitative assessment and global mapping of supercritical CO_2 power cycle technology. *Sustainable Energy Technologies and Assessments*. 2021; 43: 100978. Available from: https://doi.org/10.1016/j.seta.2020.100978.

[4] Dalkic G, Balaban O, Tuydes-Yaman H, Celikkol-Kocak T. An assessment of the CO_2 emissions reduction in high speed rail lines: two case studies from Turkey. *Journal of Cleaner Production*. 2017; 165: 746–761. Available from: https://doi.org/10.1016/j.jclepro.2017.07.045.

[5] Valone TF. Gigatonne carbon dioxide removal can reverse global heating trend. *Asian Journal of Environment and Ecology*. 2023; 20(2): 42–58. Available from: https://www.sdiarticle5.com/review-history/97404.

[6] Fawcett D, Sitch S, Ciais P, Wigneron JP, Silva-Junior CH, Heinrich V, et al. Declining Amazon biomass due to deforestation and subsequent degradation losses exceeding gains. *Global Change Biology*. 2023; 29(4): 1106–1118. Available from: https://doi.org/10.1111/gcb.16513.

[7] Zastrow M. China's tree-planting could falter in a warming world. *Nature*. 2019; 573(7775): 474–475. Available from: https://doi.org/10.1038/d41586-019-02789-w.

[8] Datta S. Continuing the forest conservation debate: rhetoric and reality of green India mission. *Economic and Political Weekly*. 2016; 51(4): 49–55. Available from: https://www.jstor.org/stable/44003108.

[9] Fry I. Reducing emissions from deforestation and forest degradation: opportunities and pitfalls in developing a new legal regime. *Review of European Community and International Environmental Law*. 2008; 17(2): 166–182. Available from: https://doi.org/10.1111/j.1467-9388.2008.00597.

[10] Azam M, Raza A. Does foreign direct investment limit trade-adjusted carbon emissions: fresh evidence from global data. *Environmental Science and Pollution Research*. 2022; 29(25): 37827–37841. Available from: https://doi.org/10.1007/s11356-021-18088-9.

[11] Sun M, Liang B, Meng X, Zhang Y, Wang Z, Wang J. Study on the evolution of spatial and temporal patterns of carbon emissions and influencing factors in China. *Land*. 2024; 13(6): 828. Available from: https://doi.org/10.3390/land13060828.

[12] Amin P, Memarian A, Repo E, Andersson M, Mansouri SS, Zendehboudi S, et al. Mathematical modeling of dispersed CO_2 dissolution in ionic liquids: application to carbon capture. *Journal of Molecular Liquids*. 2024; 402: 124486. Available from: https://doi.org/10.1016/j.molliq.2024.124486.

[13] Hameed G, Nair PN, Tan RR, Foo DC, Short M. A novel mathematical model to incorporate carbon trading and other emission reduction techniques within energy planning models. *Sustainable Production and Consumption*. 2023; 40: 571–589. Available from: https://doi.org/10.1016/j.spc.2023.07.022.

[14] Wu Y, Zhang H, Wang S, Zhen L. Mathematical optimization of carbon storage and transport problem for carbon capture, use, and storage chain. *Mathematics*. 2023; 11(12): 2765. Available from: https://doi.org/10.3390/math11122765.

[15] Peng J, Xia B, Guo W. Multi-scale dynamic mathematical model of CO_2 and fly ash mineralization. *Journal of Cleaner Production*. 2023; 425: 139054.

[16] Jha A, Misra AK. Consequences of shifting to renewable energy on atmospheric carbon dioxide: a mathematical model. *Journal of Applied Mathematics and Computing*. 2024; 70(5): 4851–4876. Available from: https://doi.org/10.1007/s12190-024-02149-6.

[17] Khan H, Rajpar AH, Alzabut J, Aslam M, Etemad S, Rezapour S. On a fractal-fractional-based modeling for influenza and its analytical results. *Qualitative Theory of Dynamical Systems*. 2024; 23(2): 70. Available from: https://doi.org/10.1007/s12346-023-00918-5.

[18] Khan H, Alzabut J, Gómez-Aguilar JF, Alfwzan WF. A nonlinear perturbed coupled system with an application to chaos attractor. *Results in Physics*. 2023; 52: 106891. Available from: https://doi.org/10.1016/j.rinp.2023.106891.

[19] Coronel-Escamilla A, Solís-Pérez JE, Gómez-Aguilar JF, Razo-Hernández JR, Alderremy AA, Aly S. Dynamics and synchronization of a fractional conformable neural network with power-law. *The European Physical Journal Special Topics*. 2022; 231(10): 1771–1788. Available from: https://doi.org/10.1140/epjs/s11734-022-00465-1.

[20] Viera-Martin E, Gómez-Aguilar JF, Solís-Pérez JE, Hernández-Pérez JA, Escobar-Jiménez RF. Artificial neural networks: a practical review of applications involving fractional calculus. *The European Physical Journal Special Topics*. 2022; 231(10): 2059–2095. Available from: https://doi.org/10.1140/epjs/s11734-022-00455-3.

[21] Yao Z, Sun K, He S. Synchronization in fractional-order neural networks by the energy balance strategy. *Cognitive Neurodynamics*. 2024; 18(2): 701–713. Available from: https://doi.org/10.1007/s11571-023-10023-7.

[22] Cao J, Udhayakumar K, Rakkiyappan R, Li X, Lu J. A comprehensive review of continuous-/discontinuous-time fractional-order multidimensional neural networks. *IEEE Transactions on Neural Networks and Learning Systems*. 2021; 34(9): 5476–5496. Available from: https://doi.org/10.1109/TNNLS.2021.3129829.

[23] Ge C, Zhang Q, Wang H, Wang L. Order-dependent sampling control for state estimation of uncertain fractional-order neural networks system. *Optimal Control Applications and Methods*. 2024; 45(2): 758–770. Available from: https://doi.org/10.1002/oca.3071.

[24] Khan A, Abdeljawad T, Alqudah MA. Neural networking study of worms in a wireless sensor model in the sense of fractal fractional. *AIMS Mathematics*. 2023; 8(11): 26406–26424. Available from: https://doi.org/10.3934/math.20231348.

[25] Chakraverty S, Jena RM, Jena SK. *Time-Fractional Order Biological Systems with Uncertain Parameters*. Synthesis Lectures on Mathematics and Statistics. Springer; 2023.

[26] Yogeesh N, Mohammad SI, Divyashree J, Raja N, Vasudevan A, Long H. Pesticide residue induced hepatotoxicity: determination for animal studies based on fuzzy logic. *Applied Mathematics*. 2025; 19(2): 365–378. Available from: https://doi.org/10.18576/amis/190212.

[27] Farman M, Talib A, Nisar KS, Sambas A, Bayram M, Hafez M. Investigation of ABPV predict dynamics infection in honeybee colony production: soft patterns multiscale modeling with fractional approach. *Ain Shams Engineering Journal*. 2025; 16(10): 103626.

[28] Atici FM, Eloe P. Discrete fractional calculus with the nabla operator. *Electronic Journal of Qualitative Theory of Differential Equations*. 2009; 2009: 3. Available from: http://eudml.org/doc/227223.

[29] Abdeljawad T, Baleanu D. Discrete fractional differences with nonsingular discrete Mittag-Leffler kernels. *Advances in Difference Equations*. 2016; 2016(1): 1–22. Available from: https://doi.org/10.1186/s13662-016-0949-5.

[30] Abdeljawad T. On Riemann and Caputo fractional differences. *Computers and Mathematics with Applications*. 2011; 62(3): 1602–1611.

[31] Ran J. Discrete chaos in a novel two-dimensional fractional chaotic map. *Advances in Difference Equations*. 2018; 2018(1): 294. Available from: https://doi.org/10.1186/s13662-018-1760-2.

[32] Selvam AG, Alzabut J, Dhineshbabu R, Rashid S, Rehman M. Discrete fractional order two-point boundary value problem with some relevant physical applications. *Journal of Inequalities and Applications*. 2020; 2020: 1–9. Available from: https://doi.org/10.1186/s13660-020-02485-8.

[33] Caetano MA, Gherardi DF, Yoneyama T. An optimized policy for the reduction of CO_2 emission in the Brazilian Legal Amazon. *Ecological Modelling*. 2011; 222(15): 2835–2840. Available from: https://doi.org/10.1016/j.ecolmodel.2011.05.003.

[34] Misra AK, Verma M. A mathematical model to study the dynamics of carbon dioxide gas in the atmosphere. *Applied Mathematics and Computation*. 2013; 219(16): 8595–8609. Available from: https://doi.org/10.1016/j.amc.2013.02.058.

[35] Devi S, Gupta N. Dynamics of carbon dioxide gas (CO_2): effects of varying capability of plants to absorb CO_2. *Natural Resource Modeling*. 2019; 32(1): e12174. Available from: https://doi.org/10.1111/nrm.12174.

[36] Zhang Y, Guo H, Xiong X. Forecasting Chinese carbon emissions from fossil energy based on the fractional order cumulative multivariate grey model. *Journal of Mathematics*. 2022; 2022(1): 5623519. Available from: https://doi.org/10.1155/2022/5623519.

[37] Elsonbaty AM, Sabir Z, Ramaswamy R, Adel W. Dynamical analysis of a novel discrete fractional SITRS model for COVID-19. *Fractals*. 2021; 29(8): 2140035. Available from: https://doi.org/10.1142/S0218348X21400351.

[38] He ZY, Abbes A, Jahanshahi H, Alotaibi ND, Wang Y. Fractional-order discrete-time SIR epidemic model with vaccination: chaos and complexity. *Mathematics*. 2022; 10(2): 165. Available from: https://doi.org/10.3390/math10020165.

[39] Yue H, Bu L. Prediction of CO_2 emissions in China by generalized regression neural network optimized with fruit fly optimization algorithm. *Environmental Science and Pollution Research*. 2023; 30(33): 80676–80692. Available from: https://doi.org/10.1007/s11356-023-27888-0.

[40] Qu H, Liu X, She Z. Neural network method for fractional-order partial differential equations. *Neurocomputing*. 2020; 414: 225–237. Available from: https://doi.org/10.1016/j.neucom.2020.07.063.

[41] Aguilar CZ, Gómez-Aguilar JF, Alvarado-Martínez VM, Romero-Ugalde HM. Fractional order neural networks for system identification. *Chaos, Solitons and Fractals*. 2020; 130: 109444. Available from: https://doi.org/10.1016/j.chaos.2019.109444.

[42] Jahanbakhti H. A novel fractional-order neural network for model reduction of large-scale systems with fractional-order nonlinear structure. *Soft Computing*. 2020; 24(17): 13489–13499. Available from: https://doi.org/10.1007/s00500-020-04763-5.

[43] Yan Z, Zhong S, Lin L, Cui Z. Adaptive Levenberg-Marquardt algorithm: a new optimization strategy for Levenberg-Marquardt neural networks. *Mathematics*. 2021; 9(17): 2176. Available from: https://doi.org/10.3390/math9172176.

[44] Arif J, Chaudhuri NR, Ray S, Chaudhuri B. Online Levenberg-Marquardt algorithm for neural network based estimation and control of power systems. In: *Proceedings of the 2009 International Joint Conference on Neural Networks*. IEEE; 2009. p.199–206.

[45] Lera G, Pinzolas M. Neighborhood based Levenberg-Marquardt algorithm for neural network training. *IEEE Transactions on Neural Networks*. 2002; 13(5): 1200–1203. Available from: https://doi.org/10.1109/TNN.2002.1031951.

[46] Labzovskii LD, Mak HW, Kenea ST, Rhee JS, Lashkari A, Li S, et al. What can we learn about effectiveness of carbon reduction policies from interannual variability of fossil fuel CO_2 emissions in East Asia? *Environmental Science and Policy*. 2019; 96: 132–140. Available from: http://hdl.handle.net/10722/283085.

[47] Yasin F, Afzal Z, Saleem MS, Jahangir N, Shang Y. Hermite-Hadamard type inequality for non-convex functions employing the Caputo-Fabrizio fractional integral. *Research in Mathematics*. 2024; 11(1): 2366164. Available from: https://doi.org/10.1080/27684830.2024.2366164.

[48] Manoj N, Sriraman R, Gurusamy R, Shang Y. Further results on global stability of Clifford-valued neural networks subject to time-varying delays. *Neurocomputing*. 2025; 651: 130886. Available from: https://doi.org/10.1016/j.neucom.2025.130886.